

Air-coupled ultrasonic bending plate transducer with piezoelectric and electrostatic transduction element combination

Matthias Rutsch¹, Omar Ben Dali¹, Axel Jäger¹, Gianni Allevalo¹,
Kai Beerstecher¹, Juliette Cardoletti¹, Aldin Radetina¹, Lambert Alff¹, and Mario Kupnik¹
¹Technische Universität Darmstadt, Germany.

Abstract—We present a simulation of an ultrasonic transducer element with piezoelectric and electrostatic transduction combined and with two bending plates. It combines the high SPL of a piezoelectric transducer with the tunable resonance frequency of a CMUT due to spring softening effect. In this work, we compare two state-of-the-art transducers with our approach: First, a piezoelectric bending plate transducer, based on a Murata MA40S4S transducer; second, a piezoelectric bending plate positioned above an additional electrode (piezoelectric and electrostatic transduction principle combined) and, third, a new structure, based on two bending plates with piezoelectric and electrostatic transduction combined (piezoelectric and electrostatic double-bending plate transducer). We use COMSOL Multiphysics 5.4 for creating a multiphysical model, including the electrical, mechanical and acoustical domain. We simulate mechanical total displacement and the directivity pattern. Thermoviscous losses in the air gap between the two bending plates are considered as well. The double-bending plate transducer has an increased amplitude of up to 570% at 80% of the pull-in voltage and a tunable resonance frequency of up to 21%. Compared to piezoelectric and electrostatic bending plate transducer, the total displacement is doubled. In addition, the radiation pattern is approximately omnidirectional, and, thus, beneficial for various applications such as obstacle detection, flow metering, distance measurement or anemometry.

Index Terms—Piezoelectric and electrostatic transduction, transducer radiation pattern, FEM.

I. INTRODUCTION

Air-coupled ultrasound in the lower frequency range of 20 kHz to 500 kHz is used in many applications such as obstacle detection, range finding, gas flow metering, anemometry or even tactile holograms. For transmission, piezoelectric bending plate transducers [Fig. 1(a), Type I] are commonly used at their resonant frequency to generate high sound pressures. Since the transmit and receive resonant frequencies differ and the transducers are generally narrow-band, they are in particular difficult to match for pulse-echo mode applications.

In contrast, electrostatic transducers without a vacuum gap, as used in many air-coupled capacitive micromachined ultrasonic transducers (CMUTs), have a more broadband frequency response. The resonance frequency can be tuned by the commonly used technique of varying the DC bias voltage [1], which is applicable for piezoelectric transducers as well [2]. Electrostatic transducers, however, feature an excellent receiving sensitivity, as exploited in capacitive microphones.

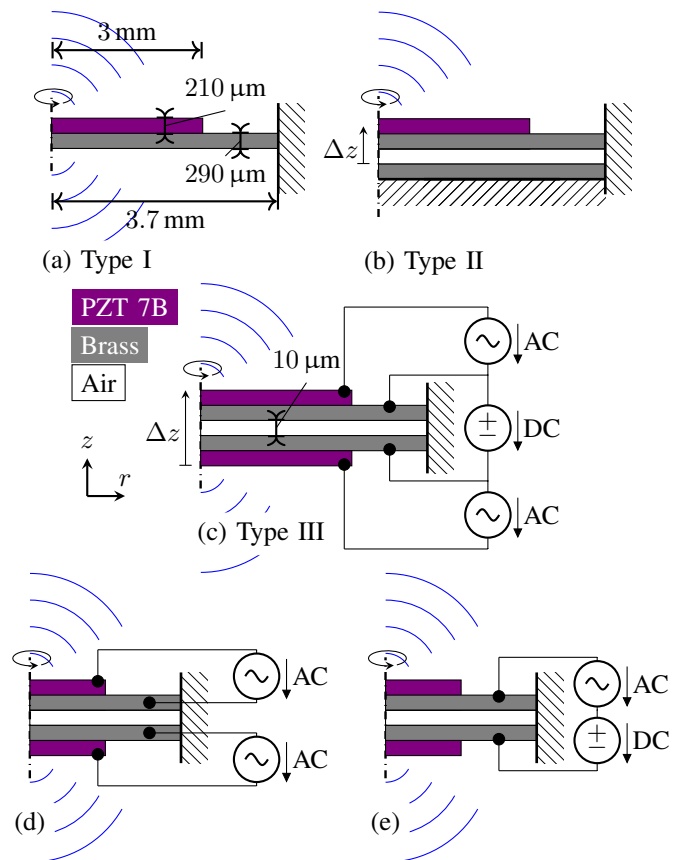


Fig. 1. The piezoelectric and electrostatic double-bending plate transducer (c) in direct comparison to the state-of-the-art transducers (a) and (b) [4]–[6]. The two bending plates (brass) have each a piezoelectric layer (PZT 7B) on top and are separated by a thin air gap of 10 μm . Note that both bending plates emit ultrasound into the surrounding medium for a more omnidirectional radiation pattern. Further, besides various biasing schemes for transmit and receive, the structure allows only piezoelectric (d) or only electrostatic transduction (e) as well.

In previous work both transduction principles, i.e. piezoelectric and electrostatic, have been combined by two different approaches: First, a piezoelectric transmitter and an electrostatic receiver are put in one single housing, e.g. [3]. Second, both transduction principles can be combined in one device as

well [4]–[6] [Fig. 1(b)], i.e. a piezoelectric and electrostatic bending plate transducer (Type II). In this approach only one bending plate is used in [4]–[6].

In this work, we introduce a piezoelectric and electrostatic double-bending plate transducer (Type III), i.e. two piezoelectric-driven bending plates are facing each other, separated by a vacuum or air gap [Fig. 1(c)]. In addition, the electrostatic transduction principle with its advantages (larger sensitivity, frequency tuning) is added by applying a DC bias voltage between the two electrically conductive plates.

In contrast to previous work [7]–[9], we propose this double-bending plate transducer to be open to both sides. In addition, note that the in [8] and [9] – so called multiple moving membrane capacitive micromachined ultrasonic transducers (M³-CMUT) – only use the electrostatic transduction principle.

Furthermore, the proposed two-sided open piezoelectric and electrostatic double-bending plate transducer (Type III) features additional various biasing schemes such as only piezoelectric-driven [Fig. 1(d)] or only electrostatic-driven [Fig. 1(e)]. In addition, the piezoelectric transduction can be used for transmit and the electrostatic transduction for receive (not shown).

In this work, we use finite element modeling (FEM) to investigate this Type III [Fig. 1(c)] transducer in comparison to Type I [Fig. 1(a)] and II [Fig. 1(b)].

II. MODELING

In order to investigate the electrical, mechanical and acoustic properties, we use an FEM. Further, this method is suitable for calculating the acoustic directivity pattern. The geometrical properties are based on a low cost ultrasonic transducer (MA40S4S, Murata, Seisakusho, Nagaokakyo, Japan) operating at 40 kHz. This transducer consists of a piezoelectric layer made of PZT 7B, a brass (CuNi₁₈Zn₂₇) plate and a metal cone for further sensitivity amplification [10]. The PZT plate has a radius of 3 mm with a thickness of 210 μm. The bending plate has a radius of 3.7 mm with a thickness of 290 μm [Fig. 1(a)].

In order to add the electrostatic transduction mechanism, we use a rigid electrode positioned at a distance of 5 μm from the bending plate. This allows us to investigate the spring softening effect of Type II transducer, that varies the resonance frequency and amplitude of the total displacement Δz [Fig. 1(b)]. We define the total displacement Δz between the rigid electrode and the bending plate.

Next, we add a second bending plate, resulting in the Type III transducer [Fig. 1(c)]. The air gap between the plates is 10 μm. Each PZT element is driven with an AC voltage and the bending plates are DC biased. Here we define the total displacement Δz between the two bending plates.

We use the electrostatic, the solid mechanics, the pressure acoustics and the thermoviscous package provided by COMSOL to calculate the electrostatic and piezoelectric transduction. The equations of these packages are discussed in the following paragraphs in more detail.

In our model, the AC and DC excitation are isolated from each other, preventing the PZT layer from being prestressed by the DC biasing [2]. This is achieved by adding an artificial isolation layer in the bending plate. We split each bending plate into three equal thick layers. The electrical calculations are performed in the first and third layer only, neglecting the middle layer in the electrostatic interface. In contrast, the mechanical simulation still considers all three layers of the bending plate.

The mechanical displacement u is calculated in the frequency domain, i.e.

$$-\rho\omega^2u = \nabla \cdot (P)^T + F_V e^{i\phi}, \quad (1)$$

where ρ is the density, ω is the angular frequency, ∇ is the nabla operator, P is the first Piola-Kirchhoff stress, F_V is the volume force and the circumferential position of the volume force ϕ [12]. The mechanical properties of the bending plate are derived from [13].

The interaction of the solid mechanics interface and the electrostatics interface is analyzed using the electromechanical forces module in COMSOL, which computes the electromagnetic stress tensor σ_{EM} , i.e.

$$\sigma_{EM} = \varepsilon_0 E \otimes E - \frac{1}{2} (\varepsilon_0 E \cdot E) I, \quad (2)$$

where ε_0 is the permittivity, E is the electric field and I is the identity matrix [12].

Mechanical properties of the piezoelectric layer are computed using the constitutive equations for large deformation piezoelectricity, i.e.

$$S = c_E \varepsilon_G - e^T E \quad (3)$$

$$P_m = e \varepsilon_G + \varepsilon_0 (\varepsilon - I) E, \quad (4)$$

where S is the second Piola-Kirchhoff stress, ε_G is the Green-Lagrange strain, P_m is the electric polarization, e is the compliance matrix, c_E is the piezoelectric coupling coefficient matrix and ε is the relative permittivity [12].

According to [14], we use for the compliance matrix of PZT 7B

$$C = \begin{pmatrix} 16.7 & -5.9 & -7.5 & 0 & 0 & 0 \\ -5.9 & 16.7 & -7.5 & 0 & 0 & 0 \\ -7.5 & -7.5 & 18.8 & 0 & 0 & 0 \\ 0 & 0 & 0 & 38.8 & 0 & 0 \\ 0 & 0 & 0 & 0 & 38.8 & 0 \\ 0 & 0 & 0 & 0 & 0 & 45.4 \end{pmatrix} \cdot 10^{-12} \frac{1}{Pa}. \quad (5)$$

The acoustics in our model is computed using two different physics domains provided by COMSOL. We calculate the far field using the pressure acoustics package. This is based on the Helmholtz equation in the frequency domain, i.e.

$$\nabla \cdot \left(-\frac{1}{\rho} \nabla p_t \right) - \frac{\omega^2}{c^2 \rho} p_t = 0, \quad (6)$$

where p_t is the total pressure and c is the speed of sound [12]. The transducer is simulated assuming the pressure released state (Fig. 2).

TABLE I
USED MATERIAL PARAMETERS OF PZT 7B AND CuNi18Zn27, WHERE ρ IS THE DENSITY, ε IS THE RELATIVE PERMITTIVITY, ν IS THE POISSON'S RATIO AND E_{33} IS THE YOUNG'S MODULUS .

	PZT 7B	CuNi18Zn27
ρ (kg/m ³)	8000	8700
ε	3200	/
ν	0.36	0.34
E_{33} (GPa)	53.2	135

In order to consider the acoustic damping effects such as thermal or viscous losses, we use the thermoviscous acoustics module. It is based on the linearized Navier-Stokes equation and solves both the continuity equation and the energy equation, i.e.

$$i\omega\rho_t + \nabla(\rho u_t) = 0 \quad (7)$$

$$i\omega\rho u_t = \quad (8)$$

$$\nabla \left[-p_t I + \mu \left(\nabla u_t + (\nabla u_t)^T \right) - \left(\frac{2}{3}\mu - \mu_B \right) (\nabla u_t) I \right] + \nabla(k\nabla T_t) + Q = \quad (9)$$

$$\rho_0 C_p (i\omega T_t + u_t \nabla T_0) - \alpha_p T_0 (i\omega p_t + u_t \nabla p_0),$$

where ρ_t is the total density, u_t is the velocity field, μ is the dynamic viscosity, μ_B is the bulk viscosity, k is thermal conductivity, T_t is total temperature, Q is an additional heat source, C_p is heat capacity of constant pressure, T_0 is ambient temperature and α_p is coefficient of thermal expansion. These properties are predefined by COMSOL. The acoustic domains (pressure acoustics and thermoviscous acoustics) and the mechanical domain are coupled via the normal velocity [12]. The material properties required are summarized in Table I.

In order to simulate the ultrasonic transducer in the free field, a perfectly matched layer (PML) is required. This region is meshed using rectangular elements. In radial direction, the number of elements is set to eight (Fig. 2). The far field region is meshed with an element size of $\lambda/10$. Due to the shape of the sphere, the air is meshed using triangular elements, while the transducer is meshed with rectangular elements.

The frequency response of the prestressed transducer is calculated in two steps: First, we simulate the prestress caused by the DC voltage. Second, the biased system is simulated in the frequency domain. In order to consider geometric nonlinearities (stress stiffening) [15] as well, we use a large signal analysis including nonlinearities.

III. RESULTS AND DISCUSSION

The simulation of the Type I transducer exhibits a targeted resonance frequency of 45.95 kHz with a maximum displacement of 0.79 μm at the center of the PZT plate [Fig. 3(a)]. By introducing an electrode (Type II), both, the resonance frequency and the displacement magnitude remain constant. However, by applying a DC bias, the resonance frequency decreases while the displacement increases, as described in previous studies [8], [9]. At 80% of the pull-in voltage, we observe an SPL up to 120 dB at the tuned resonance frequency,

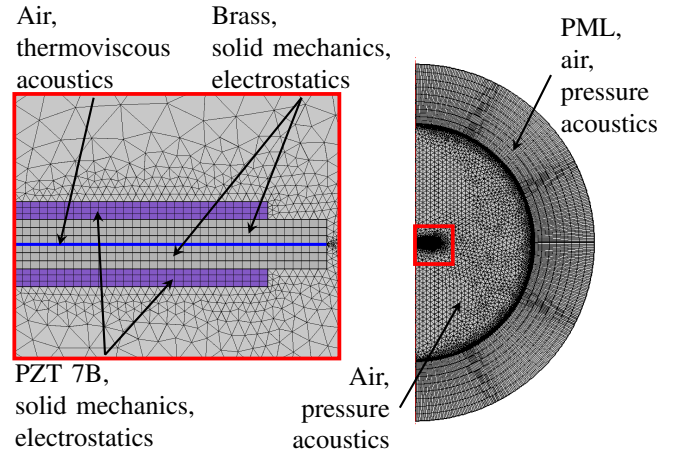


Fig. 2. The COMSOL model of the piezoelectric and electrostatic double-bending plate transducer considers the electrical and mechanical properties of both the PZT and the bending plates. The air gap between the plates is modeled using thermoviscous acoustics. The far field calculation uses the pressure acoustic package of COMSOL. A PML attenuates all incident waves of the transducers

due to the spring softening effect. The tuned resonance frequency differs from the original frequency by 21%. The effect of the DC voltage on the displacement of the electrode has to be considered. In fact, the displacement increases by 570% [Fig. 3(a)] compared to the single element transducer.

The total displacement of Type III transducer is twice the total displacement of the Type II transducer, due to the two PZT layers. The resonance frequency of the Type II transducer decreases by 21% and the displacement increases by 570% at 80% of the pull-in voltage [Fig. 3(b)]. The spring softening effect impacts both Type II and Type III the same way because we simulated the same operational point for the transducers. With just one bending plate the pull-in takes place at a displacement of 1/3 of the gap between the electrodes as expected. In the case of two bending plates, each plate can only move 1/6 of the gap before pull-in occurs. Thus, the gap of the piezoelectric and electrostatic double-bending plate transducer must be doubled in order to compare both transducer types. The pull-in voltages are 650 V for the Type II transducer and 1300 V for Type III transducer.

COMSOL is able to calculate the far field of an acoustic boundary based on the Helmholtz-Kirchhoff integral. The directivity of the Type I transducer, the Type II transducer and the Type III transducer are compared at a frequency of 40 kHz each. Each graph is normalized to its respective maximum SPL. The Type I transducer has a dipole characteristic caused by the alternating movement direction of the bending plate [Fig. 4(a)]. Thus, the pressure field in front of the transducer has a phase shift of 180° compared to the pressure field on the backside.

The Type II transducer has a more directional wave propagation [Fig. 4(b)]. The sound emitted to the back is only emitted because of the mounted electrode and the resulting diffraction. The Type III transducer is approximately omnidirectional

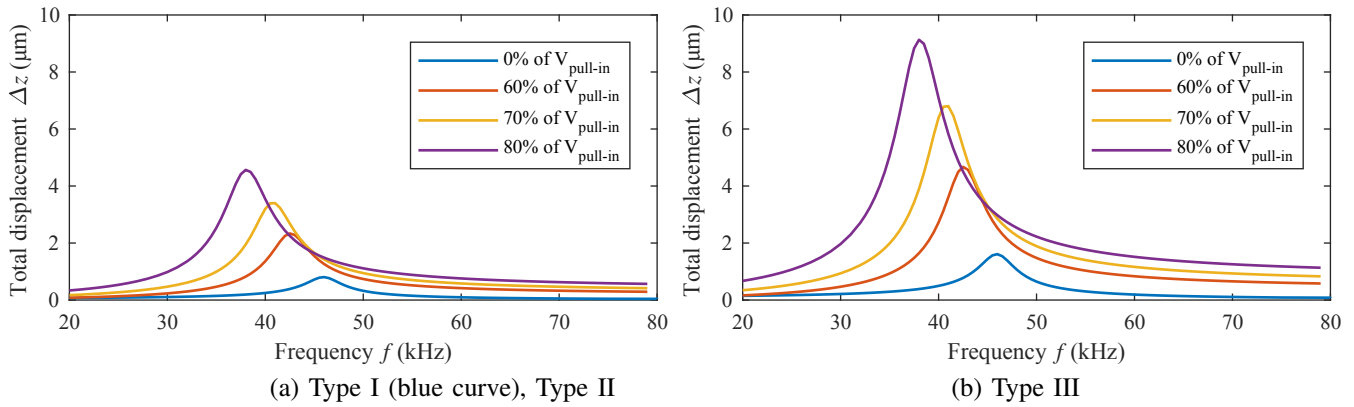


Fig. 3. If an electrode for additional electrostatic transduction [Fig. 1(b)] is used, the amplitude increases up to 570% and the resonance frequency is reduced by 21% at 80% of the pull-in voltage (a). At the same operational point, the Type III transducer [Fig. 1(c)] has the same amount of spring softening (b). Due to the two PZT layers, the total displacement is doubled. The pull-in voltages are 650 V for the piezoelectric bending plate transducer (a) and 1300 V for the piezoelectric and electrostatic double-bending plate transducer (b).

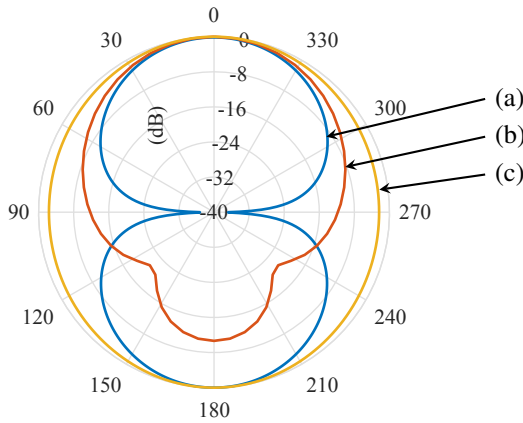


Fig. 4. Normalized radiation pattern of the Type I [Fig. 1(a)], Type II [Fig. 1(b)] and Type III [Fig. 1(c)] transducers at 40 kHz. The Type I transducer has a dipole characteristic due to the phase shift between the front pressure field and the back pressure field. The Type II transducer emits most of the acoustic energy to the front because of the fixed electrode. The Type III transducer emits ultrasound in both front and back directions, resulting in an approximately omnidirectional pattern.

[Fig. 4(c)]. Both bending plates move in opposite directions caused by the electrical excitation described in section II.

IV. CONCLUSION

Our simulation shows a piezoelectric and electrostatic double-bending plate transducer [Fig. 1(c)], emitting ultrasound with an approximately omnispherical radiation pattern.

The resonance frequency is tunable up to 21% with an increased amplitude of 570% at 80% of the pull-in voltage. At the same operational point the piezoelectric and electrostatic bending plate transducer [Fig. 1(b)] has the same change in resonance frequency and displacement but the directivity pattern is more narrow and the total displacement is halved. Applications that require an ultrasonic point source benefit from the proposed transducer.

Our next step is to manufacture a prototype of the piezoelectric and electrostatic double-bending plate transducer for

validation. In addition, we will optimize the transducer concerning the targeted resonance frequency, reduced pull-in voltage and increased SPL. Furthermore, the combination of the bottom bending plate with a Helmholtz resonator, for increased emitted acoustic energy in only one direction, will be evaluated as well. Besides that, the integration of the proposed transducer type into a 3D-printed waveguide, shown in our previous work [11], will be examined. Finally, we also plan to model the structure with an analytic lumped element model.

REFERENCES

- [1] R. Lerch, G. Sessler, and D. Wolf, *Technische Akustik: Grundlagen und Anwendungen*, Springer, 2009.
- [2] S. Loyd and J. Ming-Lin Tsai, "Electrical tuning of parameters of piezoelectric actuated transducers," U.S. Patent US2015/0358740A1, 2014.
- [3] F. Bottoni and A. Rusconi Clerici, "MEMS-Lautsprecher mit aktuatorstruktur und davon beabstandeter membran," Germany Patent DE102014106753A1, 2015.
- [4] A. L. Roest, K. Reimann, M. Klee, and J. T. M. Van Beek, "CMUTs with a high-k dielectric," U.S. Patent US2010/0202254A1, 2008.
- [5] N. A. Hall and D. Kim, "Multi-mode microphones," U.S. Patent US 2016/0219378 A1, 2015.
- [6] N. Apte, R. M. Berger, and M. Daneman, "Supplemental sensor modes and systems for ultrasonic transducer," International Patent WO2017/196678A1, 2017.
- [7] P. Robert, "Tunable bulk acoustic wave mems microsensors," U.S. Patent US2005/0162040A1, 2003.
- [8] T. A. Emadi and D. A. Buchanan, "Multiple moving membrane CMUT with enlarged membrane displacement and low pull-down voltage," *IEEE Electron Device Letters*, vol. 34, no. 12, pp. 1578–1580, 2013.
- [9] T. A. Emadi and D. A. Buchanan, "Design and characterization of a capacitive micromachined transducer with a deflectable bottom electrode," *IEEE Electron Device Letters*, vol. 36, no. 6, pp. 612–614, 2015.
- [10] *Ultrasonic sensor application manual*, Cat.no.s15e-5 ed., 2008.
- [11] A. Jäger, D. Großkurth, M. Rutsch, A. Unger, R. Golinske, H. Wang, S. Dixon, K. Hofmann, and M. Kupnik, "Air-coupled 40-khz ultrasonic 2D-phased array based on a 3D-printed waveguide structure," in Proc. *IEEE International Ultrasonics Symposium (IUS)*, pp. 1–4, 2017.
- [12] *COMSOL User's Guide*, COMSOL, 2018.
- [13] *Wieland-N17 CuNi18Zn27 C77000*, Wieland, 2014.
- [14] *PIEZOELECTRIC CERAMICS SENSORS (PIEZOTITE®)*, Cat.no.p19e-6 ed., Murata, 1997.
- [15] M. Kupnik, I. O. Wygant, and B. T. Khuri-Yakub, "Finite Element Analysis of Stress Stiffening Effects in CMUTs," in Proc. *IEEE Ultrasonics Symposium*, pp. 487–490, 2008.